Received: 1 July 2022 | Revised: 4 January 2023 | Accepted: 21 April 2023

IET Signal Processing

DOI: 10.1049/sil2.12218

The Institution of Engineering and Technology WILEY

ORIGINAL RESEARCH

Complementary waveforms for range sidelobe suppression based on a singular value decomposition approach

Jiahuan Wang[1] | Pingzhi Fan[1] | Des McLernon[2] | Zhiguo Ding[3]

[1]The School of Information Science and Technology, Southwest Jiaotong University, Chengdu, China

[2]The School of Electronic and Electrical Engineering, University of Leeds, Leeds, UK

[3]The School of Electrical and Electronic Engineering, University of Manchester, Manchester, UK

Correspondence

Pingzhi Fan.
Email: p.fan@ieee.org

Funding information

NSFC Project, Grant/Award Numbers: 62020106001, 61731017

Abstract

While Doppler resilient complementary waveforms (DRCWs) have previously been considered to suppress range sidelobes within a Doppler interval of interest in radar systems, their ability to provide Doppler resilience can be further improved. A new singular value decomposition (SVD)-based DRCW construction is proposed, in which both transmit pulse trains (made up of complementary pairs) and receive pulse weights are jointly considered. Besides, using the proposed SVD-based method, a theoretical bound is derived for the range sidelobes within the Doppler interval of interest. Moreover, based on the SVD solutions, a challenging non-convex optimization problem is formulated and solved to maximise the signal-to-noise ratio (SNR) with the constraint of low range sidelobes. It is shown that, compared with existing DRCWs, the proposed SVD-based DRCW has better Doppler resilience. Further, the new optimised SVD-based DRCW has a higher SNR while maintaining the same Doppler resilience.

KEYWORDS

Doppler shift, radar signal processing, singular value decomposition, waveform analysis

1 | INTRODUCTION

In pulsed radar systems, pulse compression technology [1, 2] has commonly been used to obtain large pulse energy, wide bandwidth, and improved range resolution. Through the use of a matched filter receiver, the returned signal reflected by a target goes through a filter matched to the reverse and conjugate version of the transmitted pulse. Then the echo signal is compressed into a short pulse which is shown in the matched filter output along with the well-known maximum SNR. However, the matched filter output also has undesired range sidelobes if the pulses are not carefully chosen. Besides, for active sensing systems such as air surveillance radars, it is a challenge to detect the illegally flying micro drones in urban regions, since the signal-to-clutter ratio (SCR) of the small moving object is usually quite poor [3]. Thus, it is a key issue for an active sensing system to suppress the sidelobes in an ultra-low level under the consideration of Doppler shift, to prevent strong scatterers from masking weak targets [3].

In order to obtain these low range sidelobes, phase coding is usually used in radar for a digital pulse compression. For a phase coded waveform, it is phase coded by a unimodular code or sequence. The matched filter output of a phase coded waveform is controlled by an aperiodic auto-correlation function of a code (sequence). For bi-phase codes, the Barker code [4] is a famous code whose aperiodic auto-correlation function has low sidelobes with only one element amplitude value. In addition, the polyphase codes proposed by Heimiller [5] and Chu [6] also have low sidelobes of aperiodic auto-correlation functions. However, it is impossible to achieve zero sidelobes of an aperiodic auto-correlation with one unimodular sequence [7]. This has resulted in the use of Golay complementary pairs in phase coding.

In radar, Golay waveforms phase coded by Golay pairs are coherently transmitted, and the returned signals are also coherently processed through the matched filter. Then the sum of the matched filter outputs has very low range sidelobes since Golay pairs have an impulse-like aperiodic autocorrelation function. But the Golay pairs are sensitive to Doppler effects

that result from the moving targets. In other words, as the inter-pulse Doppler shift changes the phase of the complementary waveforms, the matched filter outputs' sum of complementary waveforms have fairly high range sidelobes. In order to solve this problem, some methods for constructing Doppler resilient complementary waveforms (DRCW) have been proposed. These existing construction methods fall into two categories.

The first category only concerns the transmission of the basic Golay waveforms. The transmission is determined by space-time codes [7–14]. Examples of these codes that play a key role in constructing Doppler resilient Golay waveforms (pulse train) are first-order Reed-Müller codes [8]. The Prouhet-Thue-Morse (PTM) sequences [7, 12, 13], oversampled PTM sequences [9], generalised PTM sequences [10], and equal sums of powers (ESP) sequences [11]. Pezeshki et al. [7] used the Prouhet-Thue-Morse (PTM) sequence to arrange the transmission of Golay waveforms to obtain a DRCW which can almost clear range sidelobes (which are approximately equal to −80 dB) in a small Doppler resilient interval (i.e., [−0.1, 0.1] in rad). Chi et al. [9] proposed DRCWs based on the oversampled PTM sequence which can also almost clear range sidelobes not only near zero Doppler but also in all rational Doppler shifts (in rad). Tang et al. [10] designed DRCW with complete complementary codes based on the generalised PTM sequence for MIMO radar, which can significantly suppress the range sidelobes near zero Doppler. However, these above transmit-only designs do not provide a large Doppler resilient interval.

To overcome the problem of transmit-only DRCW design, the second category focuses on not only the transmission of the basic Golay waveforms but also on the weight of the receiver filter. Dang et al. [15–17] proposed the binomial design (BD) that puts binomial coefficients as the weight of the receiver filter, and alternatively transmits Golay waveforms at the transmitter. The BD method has a relatively large Doppler resilient interval, in which range sidelobes are suppressed down to almost zero. Wu et al. [18] extends Dang's idea to design a Doppler resilient complementary waveform by semi-definite programing which can obtain the weight of the receiver filter and improves the signal-to-noise ratio (SNR) without suffering high range sidelobes. Furthermore, Wu et al. [19] also considered an approach directly forcing the energy of the key term in desired spectral bands under the low modulus variation constraint and weight energy, which is solved by the majorisation minimisation (MM) method efficiently. Besides, it realizes flexible Doppler interval control and very low range sidelobes if the parameters are chosen properly.

In this paper, new constructions of DRCWs based on a singular value decomposition (SVD) method are proposed. The main contributions of this paper are listed as follows:

- An SVD-based DRCW construction is proposed, by considering both transmit pulse trains (made up of complementary pairs) and receive pulse weights.
- Based on the defined ambiguity function [17], a singular value-related upper bound is derived, indicating that our new DRCW can guarantee near-zero range sidelobes (<− 80 dB) within the specified Doppler interval of interest.
- We prove that the upper bound of range sidelobes for MM-based DRCW [19] is not lower than that of the proposed SVD-based DRCW, based on the analysis of the optimization problem (Eq. (18) in [19]). Therefore, SVD-based DRCW always outperforms MM-based DRCW with respect to Doppler resilience.
- A challenging non-convex optimization problem is formulated to maximise the signal-to-noise ratio (SNR) with the constraint of low range sidelobes. Then the non-convex optimization problem is transformed into a simpler problem based on SVD solutions, which is subsequently solved by introducing a basis selection (BS) method, and modified coordinate descent (MCD) method, resulting in BS-SVD-based DRCW and MCD-SVD-based DRCW respectively.
- The proposed methods of the SVD-based DRCWs can have lower range sidelobes and a higher peak within a broader Doppler resilient interval than the previous ones. Besides, the SNR of the proposed method is also better than the previous weighed schemes (BD, MM). Thus, the proposed SVD-based DRCWs can help detect the moving targets such as illegally flying micro drones.

1.1 | Notation

The superscripts $(\cdot)^T$, $(\cdot)^*$ and $(\cdot)^H$ denote transpose, complex conjugate, and conjugate transpose, respectively. In addition, $\circ$ denotes the Hadamard product.

2 | SIGNAL MODEL

A pair of biphase sequences $\mathbf{x}$ and $\mathbf{y}$ is called a Golay pair or a complementary pair if

$$C_x[k] + C_y[k] = 2L\delta_k, \quad k = -L+1, \ldots, 0, \ldots, L-1 \tag{1}$$

where $C_x[k]$ is the auto-correlation function of $\mathbf{x}$ at lag k, δ_k is the Kronecker delta function, and $\mathbf{x} = [x[0], x[1], \ldots, x[L-1]]^T$, $\mathbf{y} = [y[0], y[1], \ldots, y[L-1]]^T$.

In the signal model, the basic Golay complementary waveforms $s_x(t)$ and $s_y(t)$ are phase coded by the Golay complementary pair $(\mathbf{x}, \mathbf{y})$ [9, 15, 16], that is,

$$s_x(t) = \sum_{l=0}^{L-1} x[l]u(t - lT_c), \quad s_y(t) = \sum_{l=0}^{L-1} y[l]u(t - lT_c), \tag{2}$$

where $u(t)$ is a unit-energy baseband pulse shape with $0 \le t \le T_c$, and T_c is the chip length [9].

Let the vector $\mathbf{p} = [p_0, p_1, \ldots, p_{N-1}]^T$ be the characteristic vector to control the transmission of the basic Golay waveforms $s_x(t)$ and $s_y(t)$, where N is the number of pulses and $p_n = 1$ or -1. If $p_n = 1$, $s_x(t)$ is transmitted, otherwise $s_y(t)$ is transmitted. Thus the characteristic vector $\mathbf{p}$ and the basic

Golay waveforms, $s_x(t)$ and $s_y(t)$ constitute the Golay transmission waveform or complementary waveform, $Z_p(t)$, that is,

$$Z_P(t) = \sum_{n=0}^{N-1}\left(\frac{1+p_n}{2}s_x(t-nT) + \frac{1-p_n}{2}s_y(t-nT)\right), \quad (3)$$

where T denotes the pulse repetition interval (PRI).

Let the input to the matched filter be $Z_P(t)e^{j\nu t}$, where $\nu = 2\pi f_d$, and f_d is the Doppler shift in Hz. Also, $Z_P(t)e^{j\nu t}$ passes through the linear filter with impulse response $Z_W^*(-t)$, where

$$Z_W(t) = \sum_{n=0}^{N-1} w_n^*\left(\frac{1+p_n}{2}s_x(t-nT) + \frac{1-p_n}{2}s_y(t-nT)\right), \quad (4)$$

$w_n \in \mathbb{C}$ is the coefficient of receiver filter and $\mathbf{w} = [w_0, w_1, \ldots, w_{N-1}]^T$.

Then the output, that is, the cross-ambiguity function is given by

$$\chi_{P,W}(\tau, f) = \int_{-\infty}^{+\infty} Z_P(t)Z_W^*(t-\tau)e^{j2\pi f t}dt. \quad (5)$$

The radar parameters (such as chip length T_c and PRI T) are chosen to ensure that LT_c is much less than T and νLT_c is almost equal to zero, where f is the Doppler shift in Hz. After carefully choosing the radar parameters, the centre lobe of $\chi_{P,W}(\tau, \nu)$ depends on the discrete cross ambiguity function [17, 18].

$$\begin{aligned}\mathcal{A}_{P,W}(k,\theta) &= \frac{1}{2}\left[C_x[k] + C_y[k]\right]\sum_{n=0}^{N-1} w_n e^{jn\theta} \\ &+ \frac{1}{2}\left[C_x[k] - C_y[k]\right]\sum_{n=0}^{N-1} p_n w_n e^{jn\theta},\end{aligned} \quad (6)$$

where $\theta = 2\pi fT$ is the Doppler shift in radians. The complete proof is given as follows.

Proof. Consider that $s_x(t)$ is phase coded by $\mathbf{x} = [x[0], \ldots, x[L-1]]^T$, and the discrete time is $\tau = kT_c$, $k = -L+1, \ldots, L-1$, then the discrete-time ambiguity function of $s_x(t)$ is written as [20].

$$\begin{aligned}\chi_x(kT_c, f) &= \int_{-\infty}^{\infty} s_x(t)\cdot s_x^*(t+kT_c)e^{j2\pi f t}dt \\ &= \sum_{l=0}^{L-1} x[l]x^*[k+l]\cdot\frac{\sin(\pi f T_c)}{\pi f T_c}\cdot e^{j\pi f(2l-1)T_c}.\end{aligned} \quad (7)$$

Since $\pi f(2l-1)T_c < 2\pi fLT_c$, $l = 0, 1, \ldots, L-1$ and $\pi fT_c < 2\pi fLT_c$, if $2\pi fLT_c$ is almost equal to zero, that is, νLTc is almost equal to zero, and it can be proved that

$$\frac{\sin(\pi f T_c)}{\pi f T_c}\cdot e^{j\pi f(2l-1)T_c} \approx 1, \quad (8)$$

so that

$$\chi_x(kT_c, f) = \sum_{l=0}^{L-1} x[l]x^*[k+l] = C_x(k), \quad (9)$$

which means that the ambiguity function can be equivalent to the autocorrelation function. Similarly,

$$\chi_y(kT_c, f) = C_y(k). \quad (10)$$

Since the cross ambiguity function $\chi_{P,W}(\tau, f)$ for $\tau \in [-T, T]$ is written as [17].

$$\begin{aligned}\chi_{P,W}(\tau,f) &= \int_{-\infty}^{+\infty} Z_P(t)Z_W^*(t+\tau)e^{j2\pi f t}dt \\ &= \sum_{n=0}^{N-1} w_n\left[\frac{1+p_n}{2}\chi_x(\tau,f) + \frac{1-p_n}{2}\chi_y(\tau,f)\right]e^{j2\pi f nT} \\ &= \frac{1}{2}\left[\chi_x(\tau,f) + \chi_y(\tau,f)\right]\sum_{n=0}^{N-1} w_n e^{j2\pi f nT} \\ &+ \frac{1}{2}\left[\chi_x(\tau,f) - \chi_y(\tau,f)\right]\sum_{n=0}^{N-1} p_n w_n e^{j2\pi f nT},\end{aligned} \quad (11)$$

then let $\theta = 2\pi fT$, and we have

$$\begin{aligned}&\chi_{P,W}\left(kT_c, \frac{\theta}{2\pi T}\right) \\ &= \frac{1}{2}\left[\chi_x\left(kT_c, \frac{\theta}{2\pi T}\right) + \chi_y\left(kT_c, \frac{\theta}{2\pi T}\right)\right]\sum_{n=0}^{N-1} w_n e^{jn\theta} \\ &+ \frac{1}{2}\left[\chi_x\left(kT_c, \frac{\theta}{2\pi T}\right) - \chi_y\left(kT_c, \frac{\theta}{2\pi T}\right)\right]\sum_{n=0}^{N-1} p_n w_n e^{jn\theta}, \\ &= \frac{1}{2}\left[C_x(k) + C_y(k)\right]\sum_{n=0}^{N-1} w_n e^{jn\theta} \\ &+ \frac{1}{2}\left[C_x(k) - C_y(k)\right]\sum_{n=0}^{N-1} p_n w_n e^{jn\theta}.\end{aligned} \quad (12)$$

In our manuscript, notation $\mathcal{A}_{P,W}(k,\theta)$ is used to replace $\chi_{P,W}\left(kT_c, \frac{\theta}{2\pi T}\right)$, then Equation (6) holds. □

On the right-side of Equation (6), the first term only determines the shape of $|\mathcal{A}_{P,W}(0,\theta)|$ since the Golay complementary pair (**x**, **y**) makes the first term vanish at nonzero k. However, a key term $f_{\mathbf{z}}(\theta)$ in the second term results in the range sidelobes, where

$$f_{\mathbf{z}}(\theta)=\sum_{n=0}^{N-1} z_n e^{jn\theta}. \tag{13}$$

here, $z_n = p_n w_n$ and $\mathbf{z}=[z_0, z_1, \ldots, z_{N-1}]^T$. To judge the Doppler resilient complementary waveform specified by $\{\mathbf{p},\mathbf{w}\}$, two performance metrics are used, that is,

1) Doppler resilience: Let Θ be the Doppler interval of interest, then it is Doppler resilient if the range sidelobes of Equation (6) in dB are

$$20\log_{10}\left(|\mathcal{A}_{P,W}(k,\theta)|/|\mathcal{A}_{P,W}(0,0)|\right)\le -80 \text{ dB}, k\neq 0, \theta\in\Theta, \tag{14}$$

and Θ can be called the Doppler resilient interval, where the threshold -80 dB is referred from [19].

2) Signal-to-noise (SNR) [17–19]: The SNR gain produced by coherent integration is $\|\mathbf{w}\|_1^2/\|\mathbf{w}\|_2^2$, if we assume the receiver noise is Gaussian white noise. The maximum SNR gain is N, if **w** is an all-one vector.

3 | SVD APPROACH AND BOUND ANALYSIS FOR DOPPLER RESILIENCE

3.1 | SVD approach

According to [19], the Doppler interval $[-\pi, \pi)$ can be discretised into $\Phi=\{\tilde{\theta}_0,\tilde{\theta}_1,\ldots,\tilde{\theta}_{2N-1}\}$, where $\tilde{\theta}_i=\frac{2\pi(i-N)}{2N}$, $i = 0, 1, \ldots, 2N-1$. Let $\Theta\subseteq[-\pi, \pi)$ be the Doppler interval of interest. If $\tilde{\theta}_{i_m}\in\Theta$, $m = 0, 1, \ldots, M-1$, $i_m\in\{0, 1, \ldots, 2N-1\}$, then the set of Doppler shifts of interest is $\Theta_\Delta=\{\tilde{\theta}_{i_0},\tilde{\theta}_{i_1},\ldots,\tilde{\theta}_{i_{M-1}}\}$. Without loss of generality, let $\theta_m=\tilde{\theta}_{i_m}$, then we have $\Theta_\Delta = \{\theta_0, \theta_1, \ldots, \theta_{M-1}\}$. Thus, the key term Equation (13) can be transformed into a discrete form:

$$f_{\mathbf{z}}(\theta_m)=\sum_{n=0}^{N-1} z_n e^{jn\theta_m},\ m=0,1,\ldots,M-1, \tag{15}$$

which can be rewritten as a compact form:

$$f_{\mathbf{z}}(\theta_m)=\mathbf{e}_{m+1}^T\mathbf{z},\ m=0,1,\ldots,M-1, \tag{16}$$

where $\mathbf{e}_{m+1}^T=\left[e^{j0\theta_m}, e^{j1\theta_m}, \ldots, e^{j(N-1)\theta_m}\right]$.

To simply the analysis of Equation (15), a Doppler Vandermonde matrix $\mathbf{E}\in\mathbb{C}^{M\times N}$ is defined as follows:

$$\mathbf{E}=\begin{bmatrix} e^{j0\theta_0} & e^{j1\theta_0} & e^{j2\theta_0} & \cdots & e^{j(N-1)\theta_0}\\ e^{j0\theta_1} & e^{j1\theta_1} & e^{j2\theta_1} & \cdots & e^{j(N-1)\theta_1}\\ \vdots & \vdots & \vdots & \vdots & \vdots\\ e^{j0\theta_{M-1}} & e^{j1\theta_{M-1}} & e^{j2\theta_{M-1}} & \cdots & e^{j(N-1)\theta_{M-1}}\end{bmatrix}. \tag{17}$$

Then we have

$$[f_{\mathbf{z}}(\theta_0),\ldots,f_{\mathbf{z}}(\theta_{M-1})]^T=\mathbf{E}\mathbf{z} \tag{18}$$

To satisfy Equation (14), $|f_{\mathbf{z}}(\theta_m)|$ should be as small as possible which implies that $\|\mathbf{E}\mathbf{z}\|_2^2$ should be small.

Generally, singular value decomposition (SVD) of **E** is in matrix form which is given by $\mathbf{E}=\mathbf{U}\Sigma\mathbf{V}^H$, or $\mathbf{E}\mathbf{V}=\mathbf{U}\Sigma$, that is,

- if $M\le N$, we have

$$\underbrace{\mathbf{E}[\,\mathbf{v}_1\cdots\mathbf{v}_r\cdots\mathbf{v}_M\cdots\mathbf{v}_N\,]}_{\mathbf{v}\in\mathbb{C}^{N\times N}} = \underbrace{[\,\mathbf{u}_1\cdots\mathbf{u}_r\cdots\mathbf{u}_M\,]}_{\mathbf{U}\in\mathbb{C}^{M\times M}}\underbrace{\begin{bmatrix}\sigma_1 & & \\ & \ddots & \\ & & \sigma_M\end{bmatrix}}_{\Sigma\in\mathbb{C}^{M\times N}}; \tag{19}$$

where Σ in Equation (19) contains all-zero column vectors from the $(M+1)$-th column to the Nth column;
In other words,

$$\mathbf{E}\mathbf{v}_i=\begin{cases}\sigma_i\mathbf{u}_i, & \text{if}\quad i=1,2,\ldots,M\\ 0, & \text{if}\quad i=M+1,\ldots,N;\end{cases} \tag{20}$$

- if $M > N$, we have

$$\underbrace{\mathbf{E}[\,\mathbf{v}_1\cdots\mathbf{v}_r\cdots\mathbf{v}_N\,]}_{\mathbf{v}\in\mathbb{C}^{N\times N}} = \underbrace{[\,\mathbf{u}_1\cdots\mathbf{u}_r\cdots\mathbf{u}_N\cdots\mathbf{u}_M\,]}_{\mathbf{U}\in\mathbb{C}^{M\times M}}\underbrace{\begin{bmatrix}\sigma_1 & & \\ & \ddots & \\ & & \sigma_N\end{bmatrix}}_{\Sigma\in\mathbb{C}^{M\times N}} \tag{21}$$

where Σ in Equation (21) contains all-zero row vectors from the $(N+1)$-th row to the Mth row. In other words,

$$\mathbf{E}\mathbf{v}_i=\sigma_i\mathbf{u}_i,\quad i=1,2,\ldots,N. \tag{22}$$

Note that in Equations (19) and (21), **U** and **V** are unitary matrices whose 2-norms of column vectors are equal to 1 and Σ is the singular matrix whose diagonal elements are singular values.

Without loss of generality, the singular values in Equations (19) and (21) are sorted in descending order, that is, $\sigma_1 \geq \sigma_2 \geq \cdots \geq \sigma_{\min\{M,N\}}$. If $\sigma_{r+1} \approx 0$, then according to Equations (20) and (22), the desired $\mathbf{z}$ can be obtained, that is,

$$\mathbf{z} = \mathbf{v}_i, \ i = r+1, \ldots, N \tag{23}$$

which can be included in a desired matrix:

$$\mathbf{Z} = [\ \mathbf{v}_{r+1} \cdots \mathbf{v}_N\ ]. \tag{24}$$

After that, $\mathbf{p}$ and $\mathbf{w}$ can be found from $\mathbf{Z}$. Supposed that $\hat{\mathbf{z}} \in \mathbf{Z}$, then $\mathbf{p}$ and $\mathbf{w}$ are solved as follows:

$$p_n = \begin{cases} +1, & \text{if} \quad \mathrm{Re}\{\hat{z}_n\} \geq 0, \\ -1, & \text{if} \quad \mathrm{Re}\{\hat{z}_n\} < 0, \end{cases} \tag{25}$$

$$w_n = \begin{cases} +\hat{z}_n, & \text{if} \quad \mathrm{Re}\{\hat{z}_n\} \geq 0, \\ -\hat{z}_n, & \text{if} \quad \mathrm{Re}\{\hat{z}_n\} < 0. \end{cases} \tag{26}$$

Accordingly, we summarise the above approach in Algorithm 1.

Algorithm 1 The SVD-based DRCW design

1: Input $\Theta_\Delta \subseteq \Theta$, N.
2: Generate matrix $\mathbf{E}$ shown in Equation (17).
3: Do SVD of $\mathbf{E}$, obtain $\sigma_{r+1}, \ldots, \sigma_{\min\{M,N\}} < 10^{-4}$ and $\mathbf{Z} = [\mathbf{v}_{r+1}, \ldots, \mathbf{v}_N]$.
4: Select a vector from $\mathbf{Z}$, called $\hat{\mathbf{z}}$
5: Obtain $\mathbf{p}$ and $\mathbf{w}$ based on Equations (25) and (26).
6: Obtain SVD-based DRCW based on Equations (3) and (4).

3.2 | Theoretical bound

In this subsection, with respect to the proposed SVD-based DRCW, an upper bound is derived for the range sidelobes of Equation (6). Also, it is shown that the upper bound of range sidelobes of the MM-based DRCW is not lower than that of SVD-based DRCW.

In order to facilitate the derivation of the upper bound, a lemma is provided.

Lemma 1. *If $\theta \in \Theta_\Delta$, $\mathbf{E}$ is in Equation (17), then for any given $\mathbf{z} \in \mathbb{C}^N$ with $\|\mathbf{z}\|_2 = 1$, the range sidelobes of discrete-time composite ambiguity function Equation (6) can be upper bounded by $L\|\mathbf{Ez}\|_2$.*

Proof. According to Equation (18), we have

$$|f_{\mathbf{z}}(\theta)| \leq \|\mathbf{Ez}\|_2. \tag{27}$$

Then we have

$$|\mathcal{A}_{P,W}(k,\theta)| = |\frac{1}{2}\left(C_x[k] - C_y[k]\right) \sum_{n=0}^{N-1} p_n w_n e^{jn\theta}| \tag{28}$$

$$\leq L|f_{\mathbf{z}}(\theta)| \leq L\|\mathbf{Ez}\|_2. \tag{29}$$

□

Thus, we can derive an upper bound of range sidelobes of (6) for SVD-based DRCW as follows:

Proposition 1. *If $\theta \in \Theta_\Delta$, $\mathbf{E}$ is in* Equation (17), *$\mathbf{z} = \mathbf{v}_i \in \mathbf{Z}$, and the associated singular value is σ_i, then the range sidelobes of the discrete-time composite ambiguity function* Equation (6) *can be upper bounded by $L\sigma_i$.*

Proof. According to the definition of SVD, we have $\mathbf{Ev}_i = \sigma_i \mathbf{u}_i$, and based on Lemma 1, we have

$$\begin{aligned} |\mathcal{A}_{P,W}(k,\theta)| &\leq L|f_{\mathbf{z}}(\theta)| = L|f_{\mathbf{v}_i}(\theta)| \\ &\leq L\|\mathbf{Ev}_i\|_2 = L\|\sigma_i \mathbf{u}_i\|_2 = L\sigma_i. \end{aligned} \tag{30}$$

□

From Proposition 1, we know that $\sigma_i \leq 10^{-4}$ guarantees that the range sidelobes are lower than -80 dB for SVD-based DRCW if $|\mathcal{A}_{P,W}(0,0)| \geq L$.

As for the comparison of the range sidelobes of an MM-based DRCW and that of an SVD-based DRCW, let us first consider the optimization problem (Eq. (18) in [19]) to be solved by majorisation minimisation (MM), that is,

$$\begin{aligned} \min_{\mathbf{z}} \quad & \|\mathbf{Ez}\|_2^2 \\ s.t. \quad & \delta_l \leq |z_n| \leq \delta_u \\ & \|\mathbf{z}\|_2^2 = 1, \end{aligned} \tag{31}$$

where $\delta_l \leq |z_n| \leq \delta_u$ is the modulus constraint which can control SNR gain. However, the optimization problem cannot be effectively solved based on the MM framework, if matrix $\mathbf{E}$ or modulus parameters δ_l, δ_u are not chosen properly. Thus, it is necessary for us to analyse the range sidelobes of an MM-based DRCW and compare it with the proposed SVD-based DRCW.

Proposition 2. *If $\theta \in \Theta_\Delta$, $\mathbf{E}$ is in Equation (17) with $M \geq N$ and $\mathbf{z} \in \mathbb{C}^N$ with $\|\mathbf{z}\|_2 = 1$, then the upper bound of range sidelobes for an MM-based DRCW is not lower than that of the SVD-based DRCW.*

Proof. When $M \geq N$, singular value decomposition (SVD) of $\mathbf{E}$ is in matrix form which is given by $\mathbf{E} = \mathbf{U}\Sigma\mathbf{V}^H$, that is,

$$\mathbf{E} = \underbrace{[\,\mathbf{u}_1 \cdots \mathbf{u}_N \cdots \mathbf{u}_M\,]}_{\mathbf{U}\in\mathbb{C}^{M\times M}} \underbrace{\begin{bmatrix} \sigma_1 & & \\ & \ddots & \\ & & \sigma_N \end{bmatrix}}_{\Sigma\in\mathbb{C}^{M\times N}} \underbrace{[\,\mathbf{v}_1 \cdots \mathbf{v}_N\,]^H}_{\mathbf{V}^H\in\mathbb{C}^{N\times N}} \tag{32}$$

where $\mathbf{U}$ and $\mathbf{V}$ are orthogonal matrices. Then for any $\tilde{\mathbf{z}} \in \mathbb{C}^N$ and $\|\tilde{\mathbf{z}}\|_2 = 1$, we have

$$\begin{aligned} \|\mathbf{E}\tilde{\mathbf{z}}\|_2 &= \|\mathbf{U}\Sigma\mathbf{V}^H\tilde{\mathbf{z}}\|_2 = \|\Sigma\mathbf{V}^H\tilde{\mathbf{z}}\|_2 \\ &\geq \sigma_N\|\mathbf{V}^H\tilde{\mathbf{z}}\|_2 = \sigma_N\|\tilde{\mathbf{z}}\|_2 = \sigma_N. \end{aligned} \tag{33}$$

where σ_N is the smallest singular value. Based on Proposition 1, σ_N corresponds to singular vector solution $\mathbf{z} = \mathbf{v}_N$ and the range sidelobes based on SVD can be upper bounded by $L\sigma_N$. Based on Lemma 1, the range sidelobes based on MM can be upper bounded by $L\|\mathbf{E}\tilde{\mathbf{z}}\|_2$. Then based on Equation (33), we have $L\|\mathbf{E}\tilde{\mathbf{z}}\|_2 \geq L\sigma_N$. Thus, the proposed SVD-based DRCW always outperforms MM-based DRCW when Doppler resilience is considered. □

4 | DOPPLER RESILIENCE AND SNR

In this section, we consider not only Doppler resilience but also SNR, and design a DRCW based on two SVD-based approaches which will be introduced later.

The SNR is described as [15–17]:

$$\mathrm{SNR} = \frac{L\sigma_b^2}{N_0}\frac{\|\mathbf{w}\|_1^2}{\|\mathbf{w}\|_2^2}, \tag{34}$$

where σ_b^2 is the power of the target and N_0 is the power spectral density (PSD) of the white noise [17].

We can maximise the SNR by maximising the SNR gain $\|\mathbf{w}\|_1^2/\|\mathbf{w}\|_2^2$. In fact, $\|\mathbf{w}\|_1^2/\|\mathbf{w}\|_2^2$ can be replaced by $\|\mathbf{z}\|_1^2/\|\mathbf{z}\|_2^2$, because

$$\|\mathbf{z}\|_i = \|\mathbf{p}\circ\mathbf{w}\|_i = \|\mathbf{w}\|_i, \quad i = 1, 2 \tag{35}$$

where the second equation holds since $p_n = 1$ or -1.

The Doppler resilience is still considered, that is, according to Lemma 1, the range sidelobes should be controlled by

$$\|\mathbf{E}\mathbf{z}\|_2 \leq \varepsilon, \tag{36}$$

where $\mathbf{z} = \mathbf{p}\circ\mathbf{w}$, $p_n \in \{1, -1\}$. Then the optimization problem is proposed as follows:

$$\begin{aligned} \max_{\mathbf{z}} \quad & \frac{\|\mathbf{z}\|_1^2}{\|\mathbf{z}\|_2^2} \\ s.t. \quad & \|\mathbf{E}\mathbf{z}\|_2 \leq \varepsilon \end{aligned} \tag{37}$$

Although the constraint is a convex set, the optimization problem Equation (37) is still challenging, since the objective function in Equation (37) is not a concave function. To deal with it, we can transform the complex style into a much simpler form by decreasing the dimension of the optimization problem. Before transforming it, another proposition is required.

Proposition 3. *After the SVD of* $\mathbf{E}$, *the desired matrix* $\mathbf{Z}$ *is obtained as in* (24), *and* $\boldsymbol{\lambda} = [\lambda_1, \ldots, \lambda_U]^T$ *with* $\lambda_u \in [-1, 1]$, *then* $\|\mathbf{E}\mathbf{Z}\boldsymbol{\lambda}\|_2 \leq U\max_u\{\sigma_{u+r}\}$ *where* $U = N - r$.

Proof. Without loss of generality, let $\mathbf{z}_u = \mathbf{v}_{u+r}$ with $u = 1, 2, \ldots, U$. Then we can obtain that

$$\begin{aligned} \|\mathbf{E}\mathbf{Z}\boldsymbol{\lambda}\|_2 &= \left\|\mathbf{E}\left(\sum_{u=1}^{U}\lambda_u\mathbf{z}_u\right)\right\|_2 \leq \left\|\sum_{u=1}^{U}\lambda_u\mathbf{E}\mathbf{z}_u\right\|_2 \\ &\leq \sum_{u=1}^{U}|\lambda_u|\|\mathbf{E}\mathbf{z}_u\|_2 = \sum_{u=1}^{U}|\lambda_u|\|\mathbf{E}\mathbf{v}_{u+r}\|_2 \\ &= \sum_{u=1}^{U}|\lambda_u|\|\sigma_{u+r}\mathbf{u}_{u+r}\|_2 = \sum_{u=1}^{U}|\lambda_u|\|\sigma_{u+r}\|_2 \\ &\leq U\max_u\{\sigma_{u+r}\}. \end{aligned} \tag{38}$$

□

From Lemma 1 and Proposition 3, we know that the ambiguity function Equation (6) in dB can be upper bounded by $U\max_u\{\sigma_{u+r}\}$. Thus, the constraint in Equation (37) can be transformed into $\|\mathbf{E}\mathbf{Z}\boldsymbol{\lambda}\| \leq \varepsilon$ and the dimension of the optimization problem is changed from N to U where $U < N$. In other words, the original long length-N optimization variable $\mathbf{z}$ is replaced by a short length-U optimization variable $\boldsymbol{\lambda}$ so that the complexity can be decreased.

Accordingly, the new DRCW design based on solving the optimization problem, Equation (37) can be transformed into two steps:

- **Step 1.** Solve the following

$$\max_{\boldsymbol{\lambda}} \quad \frac{\|\mathbf{Z}\boldsymbol{\lambda}\|_1^2}{\|\mathbf{Z}\boldsymbol{\lambda}\|_2^2}. \tag{39}$$

- **Step 2.** Implement Equations (25) and (26) and obtain DRCW based on Equations (3) and (4).

4.1 | Basis selection (BS)-SVD-based DRCW

The optimization problem Equation (39) is still a difficult problem, since its objective function is a non-concave function with a fractional term. In this paper, a BS algorithm is

proposed which can remove the fractional expression form and transform Equation (39) into a much easier, discrete problem.

It is simple to show that if there is only one non-zero element in $\boldsymbol{\lambda}$, and it has value "1", then the optimization problem Equation (39) is transformed into

$$\max_{\boldsymbol{\lambda}} \ \|\mathbf{Z}\boldsymbol{\lambda}\|_1^2 \tag{40}$$

Therefore, among $\{\|\mathbf{z}_u\|_1 : u = 1, 2, \ldots, v, \ldots, U\}$, if $\|\mathbf{z}_v\|_1$ is the largest one, the optimal solution to Equation (40) is

$$\lambda_u = \begin{cases} 1, & \text{if } u = v \\ 0, & \text{otherwise.} \end{cases} \tag{41}$$

In other words, the so-called BS approach is to select a vector from $\mathbf{Z}$, called $\hat{\mathbf{z}}$, such that $\|\hat{\mathbf{z}}\|_1^2$ is the largest one compared with other vectors in $\mathbf{Z}$ (Algorithm 2).

Algorithm 2 Basis selection (BS)-SVD-based DRCWdesign

1: $\mathbf{z}_1, \mathbf{z}_2, \ldots, \mathbf{z}_U \in \mathbf{Z}$ are the basis vectors.
2: Compute $\|\mathbf{z}_1\|_1, \|\mathbf{z}_2\|_1, \ldots, \|\mathbf{z}_U\|_1$.
3: if $\|\mathbf{z}_u\|_1$ is the largest one, choose $\mathbf{z}_u$.
4: Let $\hat{\mathbf{z}} = \mathbf{z}_u$, then $\mathbf{p}$ and $\mathbf{w}$ can be obtained from Equations (25) and (26).
5: Obtain $\mathbf{p}$ and $\mathbf{w}$ based on Equations (25) and (26).
6: Obtain BS-SVD-based DRCW based on Equations (3) and (4).

4.2 | Modified coordinate descent (MCD)-SVD-based DRCW

Although the BS-SVD approach has a low computational complexity, it has a very limited performance because the elements of $\boldsymbol{\lambda}$ are restricted to the set $\{0, 1\}$. In order to improve the performance, we now propose another method—called the modified coordinated descent (MCD) algorithm with multiple initial points where the binary constraint on $\boldsymbol{\lambda}$ is removed and now $\lambda_u \in [-1, 1]$. MCD can be viewed as a relatively effective method to deal with the non-convex optimization problem with a much larger constraint set.

Generally speaking, the Coordinate Descent (CD) algorithms [21] are iterative methods. The most common CD algorithm is by fixing other elements of the variable vector and obtaining the new iteration point by minimising (maximising) the objective function with respect to a single element of variable vector. In other words, when an optimization problem was considered, that is,

$$\min_{\boldsymbol{x} \in \mathbb{R}^N} f(\boldsymbol{x}), \tag{42}$$

then the CD algorithm starts with some initial vector $\boldsymbol{x}^{(0)} = \left(x_0^{(0)}, x_1^{(0)}, \ldots, x_{N-1}^{(0)}\right)$ and repeats the following iteration

$$\begin{aligned}
x_0^{(k)} &= \underset{x_0}{\operatorname{argmin}} f\left(x_0, x_1^{(k-1)}, x_2^{(k-1)}, \ldots, x_{N-1}^{(k-1)}\right), \\
x_1^{(k)} &= \underset{x_1}{\operatorname{argmin}} f\left(x_0^{(k)}, x_1, x_2^{(k-1)}, \ldots, x_{N-1}^{(k-1)}\right), \\
x_2^{(k)} &= \underset{x_2}{\operatorname{argmin}} f\left(x_0^{(k)}, x_1^{(k)}, x_2, \ldots, x_{N-1}^{(k-1)}\right), \\
&\vdots \\
x_{N-1}^{(k)} &= \underset{x_{N-1}}{\operatorname{argmin}} f\left(x_0^{(k)}, x_1^{(k)}, x_2^{(k)}, \ldots, x_{N-1}\right),
\end{aligned} \tag{43}$$

where $k = 1, 2, 3, \cdots$.

Since the objective value of Equation (39) is always no less than 0, maximising it is equivalent to minimising the reciprocal, that is,

$$\min_{\boldsymbol{\lambda}} \ \frac{\|\mathbf{Z}\boldsymbol{\lambda}\|_2^2}{\|\mathbf{Z}\boldsymbol{\lambda}\|_1^2}. \tag{44}$$

In the optimization problem Equation (44), the objective function is still a non-convex function, so that it is difficult for us to obtain the global optimal solution. To overcome these difficulties, an MCD algorithm is proposed, which has monotonicity to guarantee convergence.

The algorithm is based on the CD algorithm. It also starts with some initial vector $\boldsymbol{\lambda}^{(0)} = \left(\lambda_1^{(0)}, \lambda_2^{(0)}, \ldots, \lambda_n^{(0)}\right)$ and then repeats the procedure as Equation (43). For details, the following formula shows the kth itertation of uth element

$$\lambda_u^{(k)} = \underset{\lambda_u}{\operatorname{argmin}} \ g\left(\lambda_1^{(k)}, \ldots, \lambda_{u-1}^{(k)}, \lambda_u, \lambda_{u+1}^{(k-1)}, \ldots, \lambda_U^{(k-1)}\right). \tag{45}$$

where $g(\boldsymbol{\lambda}) = \|\mathbf{Z}\boldsymbol{\lambda}\|_2^2 / \|\mathbf{Z}\boldsymbol{\lambda}\|_1^2$.

However, the difference between the MCD and the general CD is that MCD generates many initial vectors. For every initial vector, we repeat the iteration procedure and obtain a solution when it satisfies the stop criteria. For all these initial vectors, we have many solutions from which we can choose the best solution that has the smallest objective value. But the MCD algorithm and the MCD-SVD-based DRCW are summarised in Algorithm 3.

Algorithm 3 Modified Coordinated Descent (MCD)-SVD-based DRCW design:

for $i = 1: N_\lambda$
  randomised initial vectors $\boldsymbol{\lambda}^{(0)}$
  for $k = 1: K$
    for $u = 1: U$
      Compute $\lambda_u^{(k)}$ as Equation (43)
    end u
    if $\|\boldsymbol{\lambda}^{(k)} - \boldsymbol{\lambda}^{(k-1)}\|_2 \le \varepsilon$; $\hat{\boldsymbol{\lambda}}_i = \boldsymbol{\lambda}^{(k)}$; end
  end k
end i
• Output $\hat{\boldsymbol{\lambda}}_i$, $i = 1, 2, \ldots, N_\lambda$ and from which choose one as the best $\boldsymbol{\lambda}$ such that Equations (44) is minimised.
• Let $\hat{\mathbf{z}} = \mathbf{Z}\boldsymbol{\lambda}$, then $\mathbf{p}$ and $\mathbf{w}$ can be obtained from Equations (25) and (26).
• Obtain MCD-SVD-based DRCW based on Equations (3) and (4).

In each iteration, with regard to the suboptimal solution of the uth variable λ_u in $\boldsymbol{\lambda}$, it can be easily shown that its time-complexity is $\mathcal{O}(N_\lambda)$, where N_λ is the number of sample points in an interval. Since the iteration number is $K = \alpha N_\lambda$ and the length of vector $\boldsymbol{\lambda}$ is $U = \beta N_\lambda$, $0 \le \alpha, \beta \le 1$, the overall time-complexity is $\mathcal{O}(N_\lambda^3)$.

5 | NUMERICAL RESULTS AND DISCUSSIONS

In this section, several numerical results are presented to illustrate the performance of the proposed SVD-based DRCW. We compare the proposed DRCW based on SVD with that based on PTM [7], BD [17] and MM [19].

Throughout this section, some parameters are chosen as follows: the number of pulses is $N = 50$, the specified Doppler interval of interest is given by $\theta \in [-2.9, 2.5]$ and the Doppler sampling resolution is π/N. The ambiguity function in dB is given by

$$\mathcal{A}_{P,W}(k,\theta)(\mathrm{dB}) = 20\log_{10}\left(|\mathcal{A}_{P,W}(k,\theta)/\mathcal{A}_{P,W}(0,0)|\right). \quad (46)$$

The Doppler profile is $\mathcal{A}_{P,W}(0,\theta)(dB)$, and the peak range sidelobe level (PRSL) is given by

$$\mathrm{PRSL}(\theta) = 20\log_{10}\left(\max_{k\neq 0}\left(|\mathcal{A}_{P,W}(k,\theta)/\mathcal{A}_{P,W}(0,0)|\right)\right). \quad (47)$$

Moreover, the Golay pair is length-64 and is given by

$$\begin{aligned}\mathbf{x} = [&1,1,1,-1,1,1,-1,1,1,1,1,-1,1,1,-1,1,\\ &1,1,1,-1,-1,-1,1,-1,1,1,1,1,-1,-1,-1,1,-1,\\ &1,1,1,-1,1,1,-1,1,-1,-1,-1,1,-1,-1,1,-1,\\ &-1,-1,-1,1,1,1,-1,1,1,1,1,-1,-1,-1,1,-1],\end{aligned} \quad (48)$$

$$\begin{aligned}\mathbf{y} = [&1,-1,1,1,1,-1,-1,-1,1,-1,1,1,1,-1,-1,-1,\\ &1,-1,1,1,-1,1,1,1,1,-1,1,1,-1,1,1,1,1,-1,1,\\ &1,1,-1,-1,-1,-1,1,-1,-1,-1,1,1,1,-1,1,-1,\\ &-1,1,-1,-1,-1,1,-1,1,1,-1,1,1,1].\end{aligned} \quad (49)$$

5.1 | Doppler resilience and SNR

The Doppler resilience can be illustrated by the ambiguity function (in Figure 1), Doppler profile (in Figure 2) and PRSL (in Figure 3) for PTM-based, BD-based, MM-based, and SVD-

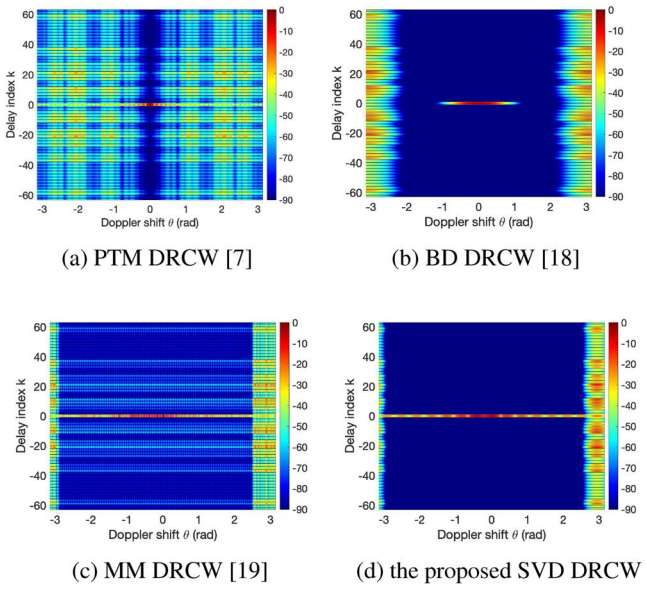

(a) PTM DRCW [7] (b) BD DRCW [18]

(c) MM DRCW [19] (d) the proposed SVD DRCW

FIGURE 1 Ambiguity functions of previous DRCW methods and the proposed SVD-DRCW method, as a function of Doppler Shift and Delay Index.

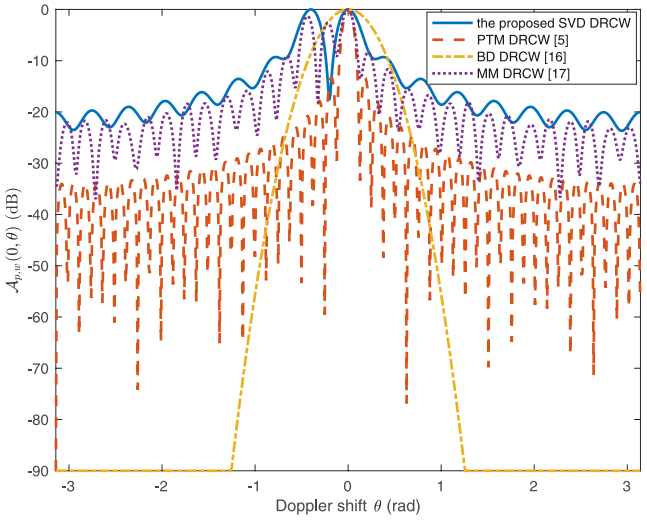

FIGURE 2 Doppler profile.

based DRCWs. Besides, the SNR gains for the proposed SVD-based DRCW and two optimised SVD-based DRCWs are shown in Figure 4.

Ambiguity Function: Figure 1 shows four ambiguity functions of the PTM-based DRCW [7], BD-based DRCW [17], MM-based DRCW [19] and the proposed SVD-based DRCW, respectively. In Figure 1a, the ambiguity function of the PTM-based DRCW has narrow Doppler resilient intervals. In Figure 1b, the ambiguity function of the BD-based DRCW has a large Doppler resilient interval, but its mainlobe $|\mathcal{A}(0,\theta)|$ reduces quickly when $|\theta| > 1$, which may result in missing fast moving targets. In Figure 1c, the ambiguity function is based on the MM method which has flexible parameter control and excellent range sidelobes suppression performance, but its range sidelobes are relatively higher than that of SVD-based DRCW. In Figure 1d which is based on the proposed SVD-based DRCW, the range sidelobes within the Doppler interval $[-2.9, 2.5]$ are no higher than -90 dB and that is an ultra low level. Besides, the mainlobe $|\mathcal{A}(0,\theta)|$ in Figure 1d always maintains a high level in the Doppler interval $\theta \in [-2.9, 2.5]$, which ensures that moving targets can be detected.

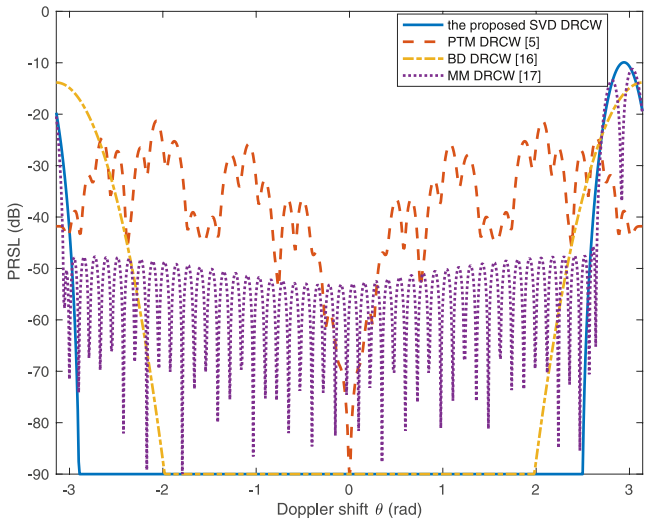

FIGURE 3 Peak range sidelobe level.

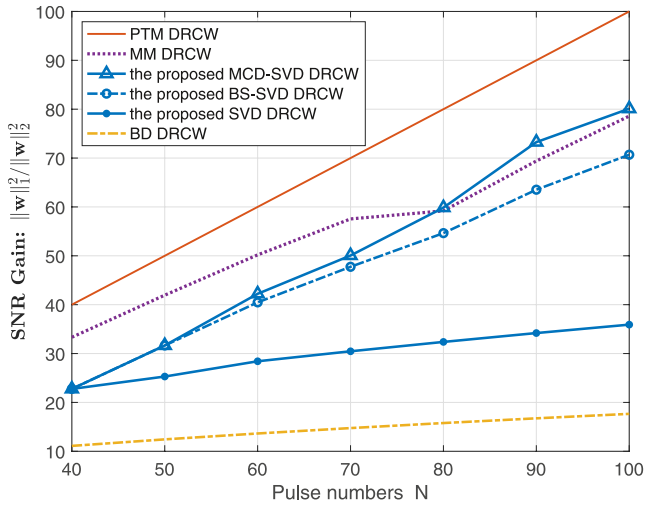

FIGURE 4 SNR gain $\left(\|\mathbf{w}\|_1^2/\|\mathbf{w}\|_2^2\right)$ versus the number of pulses N.

Doppler profile: In Figure 2, the Doppler profiles $\mathcal{A}_{P,W}(0,\theta)(\text{dB})$ versus θ based on the four schemes are compared. From Figure 2, it is observed that the Doppler profile of SVD-based DRCW has the highest level compared with the other DRCWs, which indicates that based on the proposed method, the peak of the pulse compression can be hardly masked by other sidelobes when Doppler shifts are considered.

PRSL: In Figure 3 the peak range sidelobe level (PRSL) for the four DRCWs are compared. It is obvious that the PRSL of SVD-based DRCW is the lowest one compared with the other schemes, indicating that the range sidelobes can hardly mask other targets when Doppler shifts exist.

Remark: For the MM method in [19], if we carefully set parameters in the constraint of modulus variation, the ambiguity function, Doppler profile, and the PRSL can be improved significantly, but its still worse than that of the proposed SVD-based method, as proved in Proposition 2.

SNR: In Figure 4, the SNR gains versus pulse number N for the DRCWs are compared. It can be observed that the optimised SVD DRCW (i.e., BS-SVD DRVW and MCD-SVD DRCW) significantly improve the SNR compared with the original SVD-based DRCW. Besides, the MCD-SVD DRCW has the best SNR compared with the other weighted DRCW such as the MM DRCW and BD DRCW, when pulse number $N > 80$. However, the SNRs of all weighted DRCWs are lower than the transmit-only DRCW (i.e, PTM DRCW), since higher Doppler resilience is usually achieved at the cost of SNR loss.

Summary: Above all, the proposed SVD-based DRCW has better Doppler resilience than the PTM-based, BD-based, and MM-based DRCW in the Doppler interval $[-2.9, 2.5]$. Besides, the SNR gains of the proposed BS-SVD-based DRCW and MCD-SVD-based DRCW are significantly better than the original SVD-based DRCW.

5.2 | Multiple targets with various velocities

For the scenario of multiple targets, we set the radar scene containing one stationary reflector and four moving targets with small or moderate speed. The four moving targets are 30dB weaker than the stationary reflector. The detailed parameters of these targets are given in Table 1.

TABLE 1 The parameters of targets.

	Delay index	Doppler (rad)	Relative power
Target 1	10	−1.5	−30 dB
Target 2	30	1	−30 dB
Target 3	50	0.1	−30 dB
Target 4	67	0	0 dB
Target 5	100	−0.5	−30 dB

With the parameters in Table 1, the matched filter outputs are shown in Figure 5, where the PTM-based DRCW (see Figure 5a), the BD-based DRCW (see Figure 5b), and the MM-based DRCW (see Figure 5c) are used to compare with the proposed SVD-based DRCW (see Figure 5d).

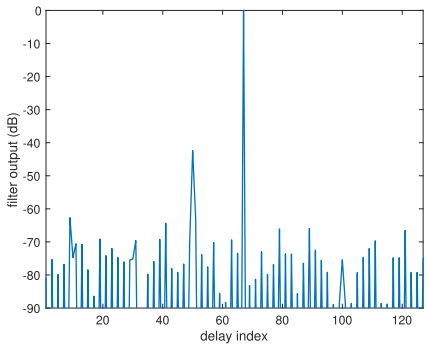

(a) PTM DRCW[7],

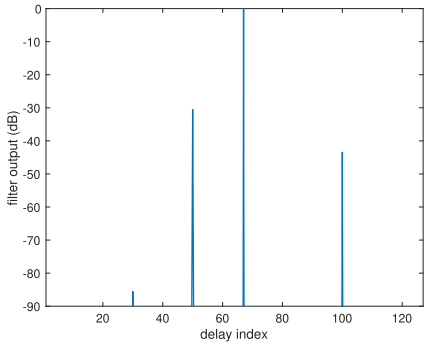

(b) BD DRCW [18],

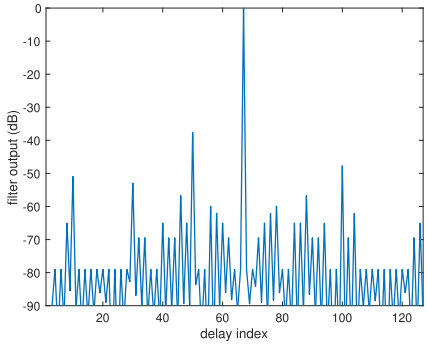

(c) MM DRCW[19],

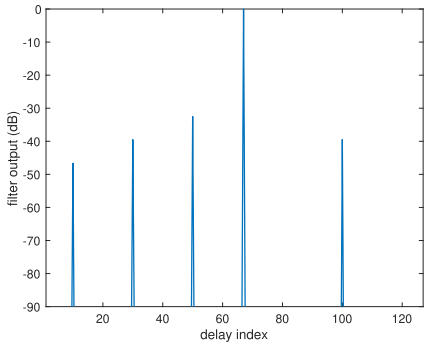

(d) Proposed SVD DRCW

FIGURE 5 The filter outputs with parameters in Table 1.

Firstly, the PTM has a very small Doppler resilient interval, in which the range sidelobes are very small. However, if the Doppler shift is outside the Doppler resilient interval, the range sidelobes are very high. From Figure 5a, it can be shown that the PTM-based DRCW has high sidelobes which mask target 1, 2, and 5 since the three targets have relatively higher Doppler shifts.

Secondly, the BD-based DRCW has a larger Doppler resilient interval than the PTM-based DRCW. From Figure 5b, it is shown that the range sidelobes are suppressed. However, target 1 is missing and target 2 is very low, which results from the fact that the range mainlobe $\mathcal{A}(0,\theta)$ is sensitive to the large Doppler shift. In other words, the range mainlobe will tend to disappear when the Doppler shift is large enough.

Thirdly, from Figure 5c, it is shown that the range sidelobes of MM-based DRCW are not suppressed thoroughly. However, it has a robust range mainlobe $|\mathcal{A}(0,\theta)|$ within the Doppler resilient interval. It can be shown in Figure 5c that the five targets can be distinguished since their amplitudes are high and the sidelobes are suppressed partly.

Fourthly, the proposed SVD also has a larger Doppler resilient interval than the PTM method. From Figure 5d, it is shown that the range sidelobes have been suppressed. Besides, it has a robust range mainlobe $|\mathcal{A}(0,\theta)|$ within the Doppler resilient interval. It can be shown in Figure 5d that the five targets are very easy to distinguish since their amplitudes are high and the sidelobes are suppressed.

6 | CONCLUSIONS

Because of the limited Doppler resilience of PTM/BD DRCW and the difficulty of choosing optimization parameters of the MM method, we have proposed an SVD-based DRCW construction, which can ensure that the discrete ambiguity function contains near-zero range sidelobes in the specified Doppler interval of interest. In addition, we use the SVD approach to analyse the ambiguity function bound which is related to the singular values. At the same time, we proved that the upper bound of the SVD DRCW is lower than the MM DRCW. Moreover, max-SNR is also considered and optimised by the BS method and MCD method which are based on the SVD solutions. Our numerical results show that, compared with the PTM-based, BD-based, and MM-based DRCW, the proposed SVD-based DRCW has better Doppler resilience performance. Finally, the optimised SVD-based DRCWs (i.e, BS-SVD-based DRCW and MCD-SVD-based DRCW) have higher SNR and the same Doppler resilience compared with the proposed SVD-based DRCW. Above all, the proposed SVD DRCWs can help the active sensing systems such as air surveillance radars to detect moving targets (e.g., illegally flying micro drones) to prevent strong scatterers from masking weak targets.

AUTHOR CONTRIBUTIONS

Jiahuan Wang: Conceptualization, Data curation, Formal analysis, Investigation, Methodology, Software, Validation, Visualization, Writing – original draft, Writing – review & editing. **Pingzhi Fan**: Funding acquisition, Project administration, Resources, Supervision, Validation, Writing – review & editing. **Des McLernon**: Writing – review & editing. **Zhiguo Ding**: Writing – review & editing.

ACKNOWLEDGEMENTS

This work was supported by NSFC Project No.62020106001/ No.61731017, and 111 project No.111-2-14.

CONFLICT OF INTEREST STATEMENT

None.

DATA AVAILABILITY STATEMENT

Data sharing not applicable to this article as no datasets were generated or analysed during the current study.

ORCID

Jiahuan Wang https://orcid.org/0000-0002-3449-6337

REFERENCES

1. Farnett, E.C., Stevens, G.H.: Pulse Compression Radar. Radar Handbook (1990)
2. Mahafza, B.R.: Radar Systems Analysis and Design Using MATLAB. CRC press (2002)
3. Wu, Z., et al.: Doppler resilient complementary waveform design for active sensing. IEEE Sensor. J. 20(17), 9963–9976 (2020). https://doi.org/10.1109/jsen.2020.2976525
4. Barker, R.H.: Group synchronizing of binary digital systems. In: Commun. Theory, pp. 273–287. Butterworth, London (1953)
5. Heimiller, R.: Phase shift pulse codes with good periodic correlation properties. IEEE Trans. Inf. Theor. 7(4), 254–257 (1961). https://doi.org/10.1109/tit.1961.1057655
6. Chu, D.C.: Polyphase codes with good periodic correlation properties. IEEE Trans. Inf. Theor. 18(4), 531–532 (1972). https://doi.org/10.1109/tit.1972.1054840
7. Pezeshki, A., et al.: Doppler resilient Golay complementary waveforms. IEEE Trans. Inf. Theor. 54(9), 4254–4266 (2008). https://doi.org/10.1109/tit.2008.928292
8. Suvorova, S., et al.: Doppler resilience, reed-müller codes and complementary waveforms. In: Conf. Rec. Forty-First Asilomar Conf. Signals, Syst., Comput., pp. 1839–1843. Pacific (2007)
9. Chi, Y.J., et al.: Range sidelobe suppression in a desired Doppler interval. In: Proc.2009 Int. Waveform Diversity Des. Conf., Kissimmee, pp. 8–13 (2009)
10. Tang, J., et al.: Construction of Doppler resilient complete complementary code in MIMO radar. IEEE Trans. Signal Process. 62(18), 4704–4712 (2014). https://doi.org/10.1109/tsp.2014.2337272
11. Nguyen, H.D., Coxson, G.E.: Doppler tolerance, complementary code sets, and generalised thue-morse sequences. IET Radar, Sonar Navig. 10(9), 1603–1610 (2016). https://doi.org/10.1049/iet-rsn.2015.0569
12. Duggal, G., et al.: Doppler-resilient 802.11 ad-based ultrashort range automotive joint radar-communications system. IEEE Trans. Aero. Electron. Syst. 56(5), 4035–4048 (2020). https://doi.org/10.1109/taes.2020.2990393
13. Wang, J., et al.: Quasi-orthogonal Z-complementary pairs and their applications in fully polarimetric radar systems. IEEE Trans. Inf. Theor. 67(7), 4876–4890 (2021). https://doi.org/10.1109/tit.2021.3063764
14. Song, X., Zhou, S., Willett, P.: Reducing the waveform cross correlation of MIMO radar with space-time coding. IEEE Trans. Signal Process. 58(8), 4213–4224 (2010). https://doi.org/10.1109/tsp.2010.2048207
15. Dang, W., et al.: 'Coordinating complementary waveforms for sidelobe suppression. In: Forty-fifth Asilomar Conf. Signals, Syst., Comput., pp. 2096–2100. Pacific (2011)
16. Dang, W.: 'Signal Design for Active Sensing', Dissertations and Theses. Gradworks (2014)
17. Dang, W., et al.: Coordinating Complementary Waveforms for Suppressing Range Sidelobes in a Doppler Band (2020). ArXiv:2001.09397
18. Wu, Z., et al.: Range-Doppler sidelobe suppression for pulsed radar based on Golay complementary codes. IEEE Signal Process. Lett. 27, 1205–1209 (2020). https://doi.org/10.1109/lsp.2020.3007093
19. Wu, Z., et al.: Design of (quasi) complementary waveform with Doppler resilience for range sidelobe suppression. In: 2020 IEEE Radar Conference (RadarConf20), pp. 1–6. Florence (2020)
20. Zhang, J., Xu, N.: Discrete phase coded sequence set design for waveform-agile radar based on alternating direction method of multipliers. IEEE Trans. Aero. Electron. Syst. 56(6), 4238–4252 (2020). https://doi.org/10.1109/taes.2020.2993683
21. Wright, S.J.: Coordinate descent algorithms. Math. Program. 151(1), 3–34 (2015). https://doi.org/10.1007/s10107-015-0892-3

How to cite this article: Wang, J., et al.: Complementary waveforms for range sidelobe suppression based on a singular value decomposition approach. IET Signal Process. e12218 (2023). https://doi.org/10.1049/sil2.12218